

Supporting Information

Unraveling Triplet Excitons Photophysics in Hyper-Crosslinked Polymeric Nanoparticles: toward the Next Generation of Solid-state Up-converting Materials

Angelo Monguzzi*¹, Michele Mauri¹, Michel Frigoli², Jacopo Pedrini¹, Roberto Simonutti¹, Chantal Larpent², Gianfranco Vaccaro¹, Mauro Sassi¹ and Francesco Meinardi*¹

¹ Dipartimento di Scienza dei Materiali, Università Milano Bicocca, via R. Cozzi 53, 20125 Milano - ITALY

² Institut Lavoisier UMR-CNRS 8180, Université de Versailles Versailles-Saint Quentin en Yvelines 45, Avenue des Etats-Unis, 78035 Versailles Cedex – FRANCE

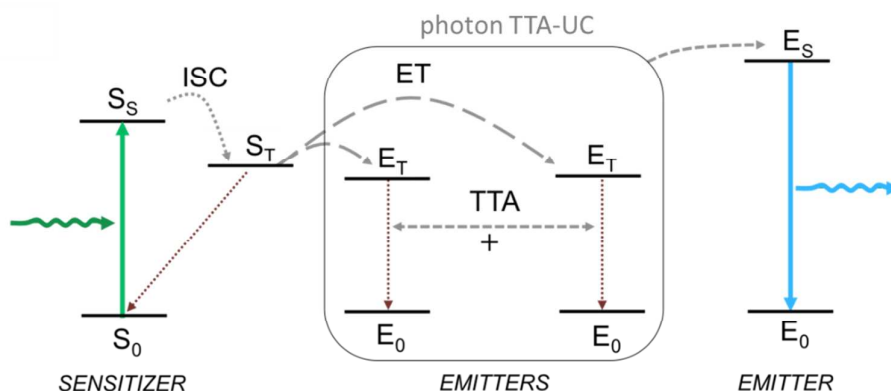


Fig. S1 Sketch of the electronic energy levels involved in the *s*TTA-UC process. Upon light absorption the sensitizers are excited into their first excited singlet state S_S and then, following intersystem crossing (ISC), to their underlying triplet state S_T . As a result of Dexter energy transfer (ET), the emitter triplets E_T are in turn excited. After E_T triplet-triplet annihilation higher energy emitter singlet states E_S are generated, whose radiative decay produces up-converted emission.

1. Synthesis of dual dye-doped polystyrene based NP

The synthesis of the polymeric NPs and the dye encapsulation have been carried out by following the procedure reported.¹ A microemulsion was prepared by progressive addition of a mixture of monomers (styrene/divinylbenzene/vinylbenzylchloride: 3.6/34.6/11.9 mmol) and 2,2-dimethoxy-2-phenylacetophenone (radical photoinitiator, 1.3 mmol) to 220 g of a 15 wt% solution of DTAB in demineralized water, under gentle magnetic stirring. The resulting microemulsion was degassed with nitrogen for 30 min and the polymerization was then carried out under white-light irradiation using two 60 W lamps, at room temperature under nitrogen, for 24 h. Chromatographic analysis indicated complete polymerization of all of the monomers. Cyclam was used in order to provide a proper stability of the nanoparticle colloidal dispersion. Cyclam-functionalized nanoparticles (NPs) were obtained by adding 1.30 g of cyclam (6.48 mmol) to 60 g of a crude suspension of the NPs. The mixture was stirred at room temperature for one week. The excess of cyclam was then removed by dialysis through a porous cellulose membrane (molecular-weight cut-off (MWCO) = 12 000 g mol⁻¹) towards an aqueous solution of DTAB (15 wt%). A stable, translucent aqueous suspension of NPs was obtained. The particle content in the suspension was about 3 wt%.

Dye doped NP-1 and NP-2 were obtained as follow : 80 µL of a DCM solution containing DPA ([DPA] = 38.58 mmol L⁻¹) and PtOEP ([PtOEP] = 0.79 mmol L⁻¹ and 1.60 mmol L⁻¹ for NP-1 and NP-2, respectively) were added to 2 mL of an aqueous suspension of the nanoparticles. The dyes permeate the NPs thanks to the swelling effect of the DCM on the crosslinked polymer. The resulting mixture was stirred at room temperature for 3 h in a capped sample tube. The tube was then uncapped and the solution was stirred for an additional 12 h to allow for the evaporation of the DCM. The suspension was filtered through a 0.2 µm MF-MilliporeTM filter before use.

The concentrations of DPA and PtOEP in the aqueous suspensions of NP1 ([DPA] = 10⁻³ M and [PtOEP] = 2x10⁻⁵ M) and NP2 ([DPA] = 10⁻³ M and [PtOEP] = 4x10⁻⁵ M) were deduced from the values of the absorbance of DPA at 374 nm ($\epsilon = 15\,500\text{ mol}^{-1}\text{ L cm}^{-1}$ in DCM) and of Soret and Q band of PtOEP at 380 nm ($\epsilon = 290\,000\text{ mol}^{-1}\text{ L cm}^{-1}$ in toluene) and 535 nm ($\epsilon = 174\,000\text{ mol}^{-1}\text{ L cm}^{-1}$ in toluene), respectively.² The average particles diameter, deduced from dynamic light scattering (DLS) is 16 nm while the atomic force microscopy (AFM) gives a slightly smaller diameter of 14 nm according to ref. 1. The particle content in the suspensions was 2.6 wt%.

The average numbers of molecules of DPA (50 in NP-1 and NP-2) and PtOEP (1 and 2 in NP-1 and NP-2, respectively) have been calculated assuming particle diameters of 8 nm and a polymer density of 1.05.g/cm³

2. Preparation of polystyrene (PS) dye-doped bulk samples.

PS bulk samples have been prepared by dissolving DPA and PtOEP in a PS:THF solution. The mixture has been stirred for 48 h under nitrogen in glove box (oxygen concentration <0.01 ppm). Later, the mixture has been kept at 50 degree on a heater to eliminate the solvent and obtain a solid bulk sample (always in controlled nitrogen atmosphere). Measurement of the sTTA-UC quantum yield have been done using a sealed cuvette in order to avoid molecular oxygen quenching.

3. sTTA-UC Quantum Yield and Threshold.

The up-conversion luminescence quantum efficiency of polymeric up-converters was determined by comparison with a DPA-PtOEP UC pair in deaerated tetrahydrofuran ([DPA] = 10 mM, [PtOEP] = 100 µM) used as secondary standard, according to the following equation:

$$QY_{uc} = QY_{std} \left(\frac{A_{std}}{A_{uc}} \right) \left(\frac{I_{uc}}{I_{std}} \right) \left(\frac{P_{std}}{P_{uc}} \right) \left(\frac{\eta_{uc}}{\eta_{std}} \right)^2 \quad \text{Eq. S1}$$

where QY , A , I , P and η represent quantum yield, absorbance at excitation intensity, integrated photoluminescence spectral profile, excitation power density, and refractive index of the medium. The subscripts “*std*” and “*uc*” indicate the reference and the sample, respectively. The UC quantum yield of the secondary standard is 0.23 at its maximum.^{3,4} The recorded spectra have been corrected for the setup optical response. The refraction index of tetrahydrofuran is 1.41 at 293 K, 1.59 for PS, and 1.33 for water.

The secondary standard solution is freshly prepared and characterized before each run of measurements. It should be noted that in the high excitation power density limit the QY_{uc} does not depend on the excitation intensity.

The PS sample have been cut into 1 mm thick slices to be encapsulated in a 1 mm optical path cuvette, the same used for the solution sample. The used setup works in a collinear geometry, which is insensitive to the position in which the photoluminescence is generated, enabling us to compare also samples with different absorbance without incurring in trivial errors.

The excitation intensity threshold has been measured by modulating the power of a CW 532 nm doubled Nd:YAG laser with a set of neutral optical filters. The excitation laser beam is Gaussian shaped, and the spot diameter containing 90% of the intensity was 340 μm . Shape and spot size have been measured by the knife-edge method.

For the pump and probe measurements, the excitation profile required has been obtained by modulating a CW 532 nm doubled Nd:YAG laser state laser at 532 nm in TTL mode, using a TTI TG5011 wavefunction generator.

4. NP Structural Characterization

A reliable picture of the NP local framework can be drawn only by using complementary techniques. The Vogel-Fulcher-Tamman-Hesse (VFTH) theory actually predicts an infinite viscosity for temperatures below the polymer glassy transition temperature (T_g). However, it must be noted that for $T < T_g$ the diffusion Stokes-Einstein relation does not hold. Nowadays, the most widely accepted scheme for the interpretation of the diffusivity of small molecules is based on the existence of spatial heterogeneity in the glassy polymers.⁴⁻⁶ At the nanometric level, small molecule mobilities can vary from region to region, thus the molecular translational diffusivity may be much larger than expected. Therefore, the investigation of the NPs requires the determination both of the T_g and of the detailed polymer dynamics, including heterogeneity. As reported in Fig 2A, the differential scanning calorimetry does not shows any phase change in the NPs up to 473 K, while, as expected, a T_g peak at 368 K is clearly visible for bulk polystyrene.⁷ This finding suggests the absence of viscous flow in the NPs even at high temperature. In fact, from stoichiometric considerations, the average weight of polystyrene chains between crosslinks points in NP is around 500 g/mol, well below 13000 g/mol of the molecular weight between entanglements for polystyrene.⁸ In order to further investigate the details of polymer dynamics we employed an advanced time domain (TD) NMR technique.⁹⁻¹⁰ Magic Sandwich Echo (MSE) TD-NMR can measure the fraction of rigid components (crystalline or glass phase) in a polymer exploiting the different mobility of the H atoms carried by the polymer chains that constitute the different phases. In the simplest case of a completely amorphous polymer, well below T_g the rigid fraction is close to unity. Any temperature increment enhances the chain mobility thus reducing the rigid fraction, until

it drops to zero over few tens of degrees above T_g . In Figure S3 the measured rigid fraction of polystyrene is depicted as function of temperature in a bulk sample.¹¹ The classical behavior described above is clearly followed: at 333 K, 30 K below the T_g , the rigid fraction starts to decrease and reaches zero at 400 K.¹² To the contrary, also the MSE TD NMR does not provide any evidence of phase transition in NP, because the rigid fraction remains essentially constant from 220 K to 420 K. Interestingly, in this temperature range a practically constant population of fast moving proton nuclei, in the range of 20%, is present, and only below 200 K the rigid fraction becomes 1. These findings are coherent with the hypercrosslinked nature of the sample: the mobile protons are associated to short strands of PS embedded within a matrix of strongly crosslinked and associated polymer chains. Thus the quantity of fast moving protons is practically constant because hypercrosslinked polymer chains can not be thermally activated into a faster moving range. On the other side, the same fixed geometry lets the local motions take place down to very low temperatures. This suggests that in highly cross-linked PS, with cross-link density 43 mol%, it is statistically possible to have relatively small cages, where phenyl rings originating from DVB do not have any translation mobility, but they can undergo unhindered rotations about their main axis. In other words they behave as molecular rotors connected to a basically immobile network acting as stator, and are able to move also at low temperature.^{13,14}

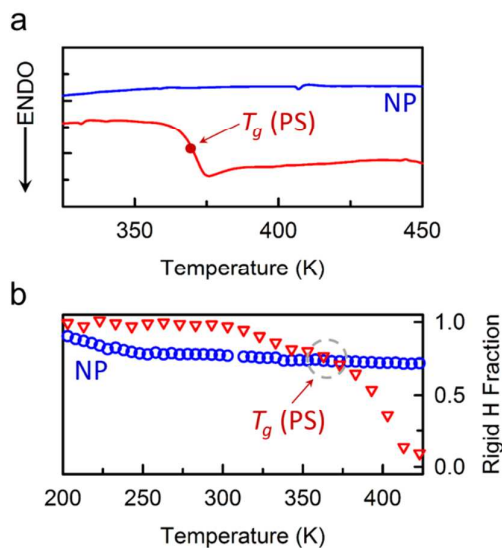


Fig. S2 (a) DSC curve of NP (dashed line) and PS (solid line) samples. (b) Rigid polymer fraction measured by TD-NMR. Error bars are smaller than the size of the dots on the graph, and represent few % points of the total.

Xenon NMR Spectroscopy. The presence of high mobility protons does not directly imply high molecular diffusion within the polymer. To determine whether this very tight network can allow any molecular diffusion we employed ^{129}Xe NMR, a technique used to characterize several systems at the nanoscale including zeolites^{15,16} polymers^{17,18}, blood¹⁹ and stones.²⁰ Fig. 2 of the main text shows the ^{129}Xe NMR spectrum of xenon in presence of pristine unloaded NPs. The gas employed for our experiment was ^{129}Xe with 26.44% natural abundance from Sapio. PS samples were placed in heavy-walled, 10 mm o.d. NMR tubes (with a 7 mm i.d.) and loosely packed to cover all the sensitive volume in the NMR coil, corresponding to a mass of around 800 mg. The sample was dehydrated overnight at 313 K under dynamic vacuum (mechanical pump, usually less than 20 Pa

i.e. 1.4×10^{-1} Torr). It was then connected to a vacuum system, and further degassed at room T and less than 8 Pa pressure (6×10^{-2} Torr). Xenon gas was initially contained in a known reservoir volume (28.29 mL), with an a pressure of 1118.6 Torr (149.13 kPa). The volume was then put in contact with the NMR tube using a Schlenk manifold. The gas was then frozen in the tube using liquid nitrogen, and the tube sealed with flame. Calculations of the final pressure of Xe in the tube are performed considering the tube internal diameter and the volume and initial pressure of the reservoir. They are then nominal pressures, neglecting the presence of the sample. ^{129}Xe NMR spectroscopy was performed using a Bruker Avance 500 system with 500.13 MHz proton resonance and 138.45 MHz ^{129}Xe resonance, equipped with a 10 mm probe. The spectrum in **Error! Reference source not found.** was acquired with single pulse excitation with $17 \mu\text{s} \pi/2$ pulse length, 20000 scans and recycle delay of 12 s.

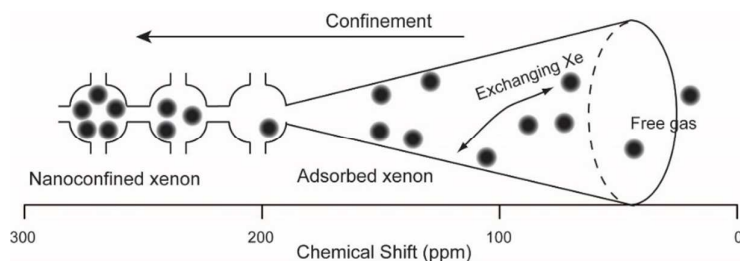


Fig. S3 General view of the relationship between confinement of ^{129}Xe nuclei and the resulting chemical shift.

There are two peaks shifted by 126 ppm and 215 ppm in respect to free gas signal that is set at zero ppm. The chemical shift value is used to estimate the free volume explored by the gas, thus describing the local environment.²¹ The most shifted peak corresponds to pores with diameter of 4.7 Å, in agreement with the values reported in literature for the free volume in bulk PS.²² The peak at 126 ppm, corresponding to spherical pores with 8.2 Å diameter, describes a second pore system which is also present in the nanoparticle and is due to the peculiar nature of hyper-crosslinked polymers. In fact, Kaliva *et al.*²³ observed by means of freeze-drying techniques that systems with at least 25 mol% of cross-linking form 7 Å pores even after solvent removal. Upon swelling, even large dye molecules (approximately 9 Å for DPA and 17 Å for PtOEP) can permeate the polymer, but after solvent removal the hyper-reticulated host envelopes the guests hindering any translational motion. The presence of two separate ^{129}Xe NMR also indicates that the mobility of xenon atoms is negligible in the NMR experiment timescale (ms) implying an even lower molecular mobility for the bigger optically active molecules. A final indication of the low translational freedom of the polymer chain is the lack of particle aggregation. This is due to the suppression of interdiffusion of polymer chains, an important mechanism of polymer adhesion.

Environment dependent photoluminescence of the AzeNaph1 Molecular Rotor. The fluorescent chromophore employed as local viscosity probe is the Donor-Acceptor derivative AzeNaph1 (Fig. 2 in the main text), whose fluorescence lifetime strongly depends upon the rotation of its electron donating and rigid dibenzoazepine residue with respect to the electron deficient naphthalene imide residue. Such rotation is progressively hindered upon increase of the local viscosity and eventually almost stopped in a rigid system.

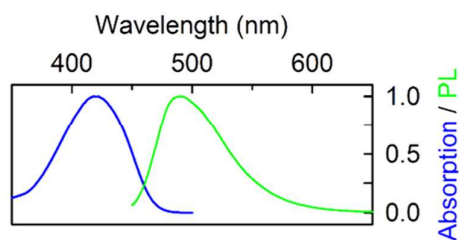


Fig. S4 Normalized absorption and PL spectrum of the molecular rotor AzeNaph1 in DMF solution.

5. Kinetics of Delayed Fluorescence upon sTTA.

Accordingly with Cheng et al.²⁴ the equation describing the evolution of the sTTA-UC intensity is

$$DF_{UC}(t) = [T]^2 \left(\frac{1 - \phi_{TTA}}{\exp[k_T t] - \phi_{TTA}} \right)^2, \quad \text{Eq. S2}$$

where ϕ_{TTA} , T , and k_T are the TTA yield, the triplet density and the triplet spontaneous decay rate, respectively.

6. Energy Transfer Efficiency Measurements.

The ET efficiencies (ϕ_{ET}) were evaluated from the measurements of the donor residual PL lifetime with (τ) and without (τ_0) the emitter as²⁵

$$\phi_{ET} = 1 - \tau / \tau_0. \quad \text{Eq. S3}$$

The PL decay traces and the corresponding ET efficiencies are reported in Fig. S5. In the case of NPs, where the PL decay is not a single exponential an average decay time was calculated as the time at which the initial PL intensity I_0 is reduced to a value I_0/e .

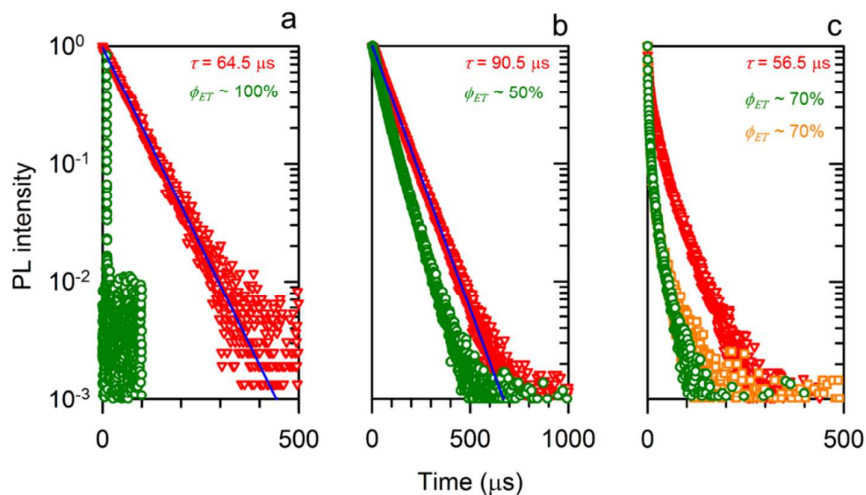


Fig. S5 Sensitizer PL decay at 645 nm under pulsed 532 nm excitation in absence (red triangles) and in presence of the emitter (green circles) in THF (a), PS (b) and NP-1, NP-2 (c, circles and squares, respectively).

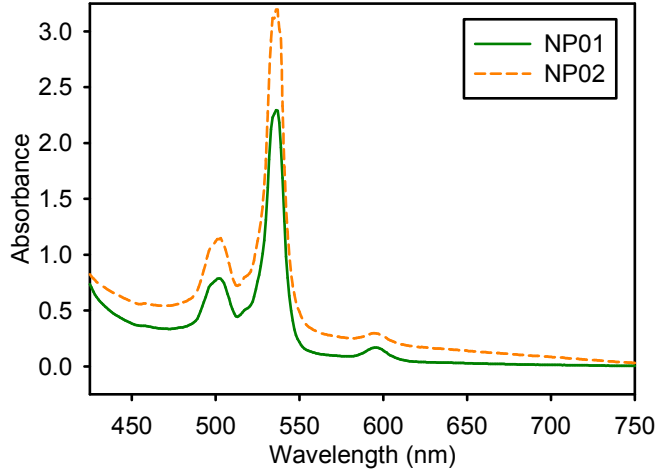


Fig. S6 Absorption spectra of NP-1 and NP-2 at normal incidence in quartz cuvette (optical path 1 cm).

7. Calculations of the TTA rate constant in hyper-reticulated NPs.

The second order annihilation rate constant (γ_{TT}) and triplet diffusion length (L) can be calculated from experimental data using the following equations:

$$I_{th} = \frac{k_T^2}{\gamma_{TT}\alpha(E)\Phi_{TTET}}, \quad (\text{Eq. S4})$$

$$\gamma_{TT} = 8\pi D a_0, \quad (\text{Eq. S5})$$

$$L = \sqrt{6 \frac{D}{k_T}}. \quad (\text{Eq. S6})$$

$\alpha(E)$ is the absorption coefficient at 532 nm determined from the absorbance of the NP, and $a_0 = 0.91$ nm is the triplet-triplet interaction radius of DPA. From Eq. S4, γ_{TT} is $3.4 \times 10^{-16} \text{ cm}^3 \text{ s}^{-1}$ and $3.2 \times 10^{-16} \text{ cm}^3 \text{ s}^{-1}$ for NP-1 and NP-2, respectively. From Eqs. S5-S6, the average triplet exciton diffusion coefficient D_T in NPs is $1.45 \times 10^{-10} \text{ cm}^2 \text{ s}^{-1}$, which gives an average triplet diffusion length of $L = 14.5 \text{ }\mu\text{m}$.

The annihilation rate k_{TTA} can be estimated using

$$k_{TTA} = \gamma_{TT}[T], \quad (\text{Eq. S7})$$

where $[T]$ is the density of triplet excitons in the system.

In NPs the minimum $[T]$ required to observe TTA is 2 exciton per NP. Considering the NP volume, $[T] = 1.39 \times 10^{18} \text{ triplets cm}^{-3}$. Therefore, the calculated value for k_{TTA} is 460 Hz, two order of magnitude higher than the measured spontaneous triplet decay rate of 4 Hz. Considering the uncertainty on the I_{th} and on the estimation of the decay rate in the case of non-exponential PL decay, this value is in good agreement with the experimental one (~ 100 Hz, Fig. 4c).

References

- (1) Gouanvé, F.; Schuster, T.; Allard, E.; Méallet-Renault, R.; Larpent, C. Fluorescence Quenching upon Binding of Copper Ions in Dye-Doped and Ligand-Capped Polymer Nanoparticles: A Simple Way to Probe the Dye Accessibility in Nano-Sized Templates. *Adv. Funct. Mater.* **2007**, *17*, 2746-2756.
- (2) Monguzzi, A.; Frigoli, M.; Larpent, C.; Tubino, R.; Meinardi, F. Low-Power-Photon Up-Conversion in Dual-Dye-Loaded Polymer Nanoparticles. *Adv. Funct. Mater.* **2012**, *22*, 139-143.
- (3) Monguzzi, A.; Tubino, R.; Hoseinkhani, S.; Campione, M.; Meinardi, F. Low power, non-coherent sensitized photon up-conversion: modelling and perspectives. *Phys. Chem. Chem. Phys.* **2012**, *14*, 4322-4332.
- (4) Cicerone, M. T.; Blackburn, F. R.; Ediger, M. D. Anomalous Diffusion of Probe Molecules in Polystyrene - Evidence for Spatially Heterogeneous Segmental Dynamics. *Macromol.* **1995**, *28*, 8224-8232.
- (5) Veniaminov, A. V.; Sillescu, H. Polymer and dye probe diffusion in poly(methyl methacrylate) below the glass transition studied by forced Rayleigh scattering. *Macromol.* **1999**, *32*, 1828-1837.
- (6) Bartko, A. P.; Xu, K. W.; Dickson, R. M. Three-dimensional single molecule rotational diffusion in glassy state polymer films. *Phys. Rev. Lett.* **2002**, *89*, 026101, 1-4.
- (7) Nguyen, H. K.; Prevosto, D.; Labardi, M.; Capaccioli, S.; Lucchesi, M.; Rolla, P. Effect of Confinement on Structural Relaxation in Ultrathin Polymer Films Investigated by Local Dielectric Spectroscopy. *Macromol.* **2011**, *44*, 6588-6593.
- (8) Fetters, L. J.; Lohse, D. J.; Richter, D.; Witten, T. A.; Zirkel, A. Connection between Polymer Molecular Weight, Density, Chain Dimensions, and Melt Viscoelastic Properties. *Macromol.* **1994**, *27*, 4639-4647.
- (9) Maus, A.; Hertlein, C.; Saalwächter, K. A Robust Proton NMR Method to Investigate Hard/Soft Ratios, Crystallinity, and Component Mobility in Polymers. *Macromole. Chem. Physic.* **2006**, *207*, 1150-1158.
- (10) Sturniolo, S.; Pieruccini, M.; Corti, M.; Rigamonti, A. Probing alpha-relaxation with Nuclear Magnetic Resonance echo decay and relaxation: A study on nitrile butadiene rubber. *Solid State Nucl. Mag.* **2013**, *51-52*, 16-24.
- (11) Mauri, M.; Dibbanti, M. K.; Calzavara, M.; Mauri, L.; Simonutti, R.; Causin, V. Time domain nuclear magnetic resonance: a key complementary technique for the forensic differentiation of foam traces. *Anal. Method.* **2013**, *5*, 4336-4344.
- (12) Tracht, U.; Wilhelm, M.; Heuer, A.; Feng, H.; Schmidt-Rohr, K.; Spiess, H. W. Length scale of dynamic heterogeneities at the glass transition determined by multidimensional nuclear magnetic resonance. *Phys. Rev. Lett.* **1998**, *81*, 2727-2730.
- (13) Gould, S. L.; Tranchemontagne, D.; Yaghi, O. M.; Garcia-Garibay, M. A. Amphidynamic character of crystalline MOF-5: Rotational dynamics of terephthalate phenylenes in a free-volume, sterically unhindered environment. *J. Am. Chem. Soc.* **2008**, *130*, 3246.
- (14) Kolokolov, D. I.; Stepanov, A. G.; Guillerm, V.; Serre, C.; Frick, B.; Jovic, H. Probing the Dynamics of the Porous Zr Terephthalate UiO-66 Framework Using H-2 NMR and Neutron Scattering. *J. Phys. Chem. C* **2012**, *116*, 12131-12136.
- (15) Cho, K.; Cho, H. S.; de Menorval, L. C.; Ryoo, R. Generation of Mesoporosity in LTA Zeolites by Organosilane Surfactant for Rapid Molecular Transport in Catalytic Application. *Chem. Mater.* **2009**, *21*, 5664-5673.
- (16) Meersmann, T.; Logan, J. W.; Simonutti, R.; Caldarelli, S.; Comotti, A.; Sozzani, P.; Kaiser, L. G.; Pines, A. Exploring single-file diffusion in one-dimensional nanochannels by laser-polarized Xe-129 NMR spectroscopy. *J. Phys. Chem. A* **2000**, *104*, 11665-11670.
- (17) Miller, J. B.; Walton, J. H.; Roland, C. M. The NMR Chemical-shift of Xe¹²⁹ Dissolved in Polymers. *Macromol.* **1993**, *26*, 5602-5610.

- (18) Simonutti, R.; Bracco, S.; Comotti, A.; Mauri, M.; Sozzani, P. Continuous flow hyperpolarized Xe-129 NMR for studying porous polymers and blends. *Chem. Mater.* **2006**, *18*, 4651-4657.
- (19) Bifone, A.; Song, Y. Q.; Seydoux, R.; Taylor, R. E.; Goodson, B. M.; Pietrass, T.; Budinger, T. F.; Navon, G.; Pines, A. NMR of laser-polarized xenon in human blood. *Proc. Natl. Acad. Sci. USA* **1996**, *93*, 12932-12936.
- (20) Mauri, M.; Simonutti, R. Hyperpolarized Xenon Nuclear Magnetic Resonance (NMR) of Building Stone Materials. *Materials* **2012**, *5*, 1722-1739.
- (21) Demarquay, J.; Fraissard, J. ¹²⁹Xe NMR of xenon adsorbed on zeolites: Relationship between the chemical shift and the void space. *Chem. Phys. Lett.* **1987**, *136*, 314-318.
- (22) Simpson, J. H.; Wen, W. Y.; Jones, A. A.; Inglefield, P. T.; Bendler, J. T. Diffusion coefficients of xenon in polystyrene determined by xenon-129 NMR spectroscopy. *Macromol.* **1996**, *29*, 2138-2142.
- (23) Kaliva, M.; Armatas, G. S.; Vamvakaki, M. Microporous Polystyrene Particles for Selective Carbon Dioxide Capture. *Langmuir* **2012**, *28*, 2690-2695.
- (24) Cheng, Y. Y.; Fückel, B.; Khoury, T.; Clady, R. G. C. R.; Tayebjee, M. J. Y.; Ekins-Daukes, N. J.; Crossley, M. J.; Schmidt, T. W. Kinetic Analysis of Photochemical Upconversion by Triplet-Triplet Annihilation: Beyond Any Spin Statistical Limit. *J. Phys. Chem. Lett.* **2010**, *1*, 1795-1799.
- (25) Inokuti, M.; Hirayama, F. Influence of Energy Transfer by the Exchange Mechanism on Donor Luminescence. *J. Chem. Phys.* **1965**, *43*, 1978-1989.